Composites Science and Technology 133 (2016) 33–39

Contents lists available at ScienceDirect

Composites Science and Technology

journal homepage: http://www.elsevier.com/locate/compscitech

In-plane strength enhancement of laminated composites via aligned carbon nanotube interlaminar reinforcement

R. Guzman de Villoria [a, 1], P. Hallander [b], L. Ydrefors [b, 2], P. Nordin [b], B.L. Wardle [a, *]

[a] Dept. of Aeronautics and Astronautics, Massachusetts Institute of Technology, Cambridge, MA, 02139, USA
[b] Saab AB, Linköping, SE 58188, Sweden

ARTICLE INFO

Article history:
Received 28 December 2015
Received in revised form
5 June 2016
Accepted 6 July 2016
Available online 13 July 2016

Keywords:
Carbon nanotubes
Structural composites
Hybrid composite
Mechanical properties
Strength

ABSTRACT

Aerospace-grade unidirectional carbon fiber laminate interfaces are reinforced with high densities (>10 billion fibers per cm^2) of aligned carbon nanotubes (A-CNTs) that act as nano-scale stitches. Such nano-scale fiber reinforcement of the ply interfaces has been shown to increase interlaminar fracture toughness and here we show that laminate in-plane strengths are also increased. Delamination damage modes associated with pre-ultimate failure are suppressed in the in-plane loaded laminates, significantly increasing load-carrying capability: tension-bearing (bolt pull out) critical strength by 30%, open-hole compression ultimate strength by 14%, and L-section bending energy and deflection by more than 25%. No increase in interlaminar or laminate thickness is observed due to the A-CNTs, but rather the ~10 nm diameter carbon nanotubes interdigitate between carbon fibers in the adjacent laminae, *i.e.*, the observed reinforcement is not due to formation of a thicker interlayer. These increases in substructural in-plane strengths are in stark contrast to degradation that typically occurs with existing 3D reinforcement approaches such as stitching, weaving and z-pinning.

1. Introduction

One of the main limitations of advanced composite materials is their poor z-direction mechanical properties due to the unreinforced pure polymer region at ply interfaces, a known Achilles heel of advanced composites. There are several approaches to reinforce such composites in the through-thickness direction including 3D weaving, stitching, and Z-pinning [1–4]. As these approaches are based on micron-diameter fibers and their assemblies (tows), in-plane fiber movement and/or damage, fiber volume loss, and stress concentrations are produced as unavoidable artifacts during manufacturing. These act to significantly reduce the in-plane mechanical properties of the laminate, such that these technologies are not in significant use [1]. Thus, the problem of weak interfaces in composites, and concomitant issues such as damage resistance and tolerance, and their implications for over-design, are outstanding limitations in composite structural performance.

In order to avoid this reduction of the in-plane properties, carbon nanotubes (CNTs) can be used as a secondary or hybrid reinforcement that can be integrated within advanced composites [5–13]. Nanomaterials, particularly carbon nanotubes (and now graphene) in their different forms, have been extensively investigated for enhancement of modulus and toughness [14–18] due to their high surface-to-volume relative to larger reinforcements, with excellent reviews available, including a specific focus on epoxies as utilized here [6,19–29]. Less work has taken on the challenge of introducing carbon nanofibers into the interlaminar region to improve mechanical properties (usually toughness). In the limited extant work, at most modest improvements are generally noted for interlaminar toughness and shear strength (*e.g.*, [30], and see review article [31]), with in-plane properties not yet being addressed [32]. Reduction in properties are primarily attributable to the low loadings (order of 1% by volume fraction) of generally low aspect ratio randomly dispersed fibers, and most improvements are likely due to an increase in interlaminar thickness through process-zone toughening. Various nanofibers and nanofillers have been investigated with the pre-dominance of work focused on CNTs. The morphology of CNTs is typically randomly dispersed, although some attempts at structured morphology interfaces have been presented, notably aligned carbon nanofibers and nanotubes grown

* Corresponding author.
E-mail address: wardle@mit.edu (B.L. Wardle).
[1] Present address: IMDEA Materials Institute, C/Eric Kandel 2, 28906, Getafe, Madrid, Spain.
[2] Present address: Exova, ASJ-vägen 7, 58254, Linköping, Sweden.

http://dx.doi.org/10.1016/j.compscitech.2016.07.006
0266-3538/

directly on microfibers (see review [11]).

Z-direction nanofibers, specifically aligned carbon nanotubes (A-CNTs), have been introduced into the interlaminar region of unidirectional composite plies in prior work (termed 'nano-stitching', see Fig. 1 [33]). The A-CNTs reinforce the interface as evidenced by steady-state fracture enhancement of 2.5–3X in Mode I and II, and importantly for the current work, do not increase the interlaminar thickness. Such toughness improvements are greater than the results reported for standard z-pinning reinforcement [1,33,34] and has the hypothesized benefit of maintaining in-plane properties due to the unobtrusive way in which the nano-scale aligned CNTs are introduced into the laminate interlaminar region. Here, we show that in-plane properties can be significantly increased, thereby giving concomitant improvement in both in-plane and out-of-plane laminate properties, in stark contrast to typical out-of-plane reinforcements (stitching, z-pinning, weaving) that degrade in-plane properties. Substructural strength tests of the type that set design limits for many practical aerospace applications, and that highlight the issue of weak interlaminar regions, include bolt-bearing (also known as tension-bearing), open hole compression (OHC) and compression after impact (CAI). Bolt-bearing and OHC failure involve mechanisms including interlaminar delamination, matrix cracking and shear, fiber microbuckling, etc [35,36]. L-shape curved laminates and other complex shapes are typical elements in aerospace structural components such as frames, co-cured webs, or angle brackets [37], and these also oftentimes fail with contributions from interlaminar modes. To explore the effectiveness of interlaminar reinforcement via A-CNTs at ply interfaces, we focus on in-plane strength evaluation including tension-bearing, OHC, and L-shape bending tests to failure.

2. Experimental

Fabrication of the laminates, including A-CNT synthesis and introduction to the laminate interfaces are first presented. This is followed by a discussion of the strength testing employed herein: bolt bearing ("filled-hole tension" or "tension bearing"), open hole compression (OHC), and L-shape bend configurations.

2.1. Aligned-CNT synthesis and laminate fabrication

A-CNTs, sometimes termed forests or vertically aligned CNTs (VACNTs), were grown in a tube furnace (Lindberg/Blue M) by chemical vapor deposition (CVD) at atmospheric pressure following procedures previously documented [38]. Si wafer pieces (30 cm × 40 cm) coated with catalyst (1/10 nm of Fe/Al_2O_3) by e-beam evaporation were placed in the quartz tube (44 mm inner diameter) reactor and pretreated at 650 °C for 7 min at reducing atmosphere (H_2/He) to condition the catalyst. A reactant mixture (H_2/He/C_2H_4) is introduced for 30 s to produce ~20 μm high A-CNTs. In order to facilitate the transfer of the forest, a reduction cycle is applied, reducing the attachment between the CNTs and the Si substrate. Further details of the process can be found elsewhere [39]. The A-CNT forests are found to have an areal density of ~1 vol% corresponding to 10^9–10^{10} CNTs per cm^2, with each CNT comprised of 3–5 walls and having an outer diameter of ~8 nm, giving an inter-CNT spacing of ~80 nm. The A-CNT forests are nominally 20 μm in length with non-trivial variability (~±10 μm) in height with extremes of 3 μm and 30 μm noted.

The A-CNT forests were introduced to the interlaminar region by manually transferring them to the surface of the composite prepreg plies. A unidirectional aerospace-grade carbon fiber and epoxy prepreg tape (Hexcel AS4/8552) was used. The prepreg material is designed to give 63.5% carbon fiber by volume and a nominal cured ply thickness of 0.130 mm in the cured laminate. The Si wafers were positioned with the CNT side in contact with the prepreg surface and moderate vacuum and heat (~1 bar and ~60 °C) was applied on each individual prepreg ply by using a vacuum bag and heating blanket assembly. Once the A-CNTs had attached to the tacky prepreg surface of a ply, the Si wafers were manually released from the attached CNT forests and the lay-up of the next ply continued until the lay-up was completed. Effectiveness of the transfer process was between ~75 and 90% of ply surface area. A standard 16-ply $[(0/90/\pm45)_2]_s$ quasi-isotropic laminate with 15 A-CNT reinforced interfaces is created. The laminates were assembled with the appropriate cure materials and cured in an autoclave following the industry process specifications (6 bar of total pressure at 1.5 °C/min to 180 °C, hold for 2 h, cool at 3 °C/min to 60 °C and vent pressure, let cool to room temperature). Baseline and A-CNT specimens were cured in the same laminate. Once the laminates (210 × 300 mm^2 in-plane dimensions) were cured, specimen edges were cut to size and prepared for the different tests. Specimen dimensions and test specifics are provided below. All of the specimens, baseline and A-CNT reinforced, had measured thickness within 1 standard deviation of the nominal 2.080 mm laminate thickness.

2.2. Laminate strength testing

Specimen configurations and testing details are described for

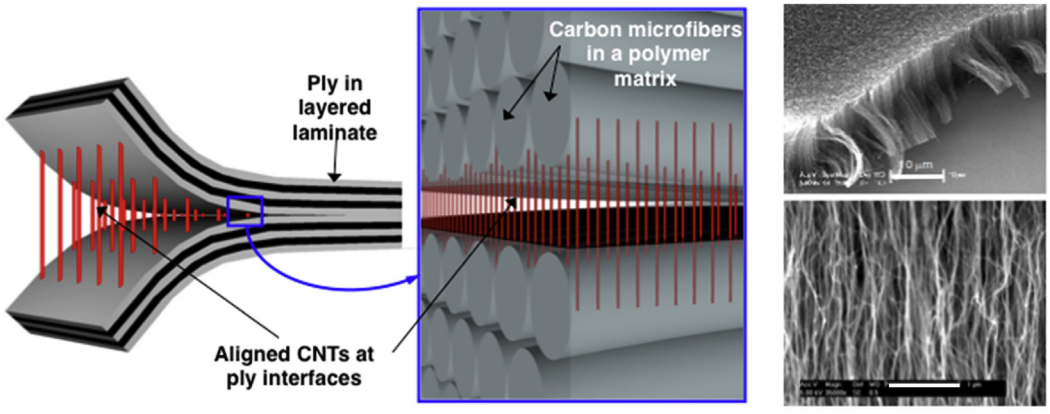

Figure 1. 'Nanostitching' concept where aligned carbon nanotubes (A-CNTs) bridge ply interfaces in laminated composites: (*left*) concept illustration of A-CNTs at a laminate interface, and (*right*) scanning electron micrographs of representative A-CNT forests showing CNT alignment.

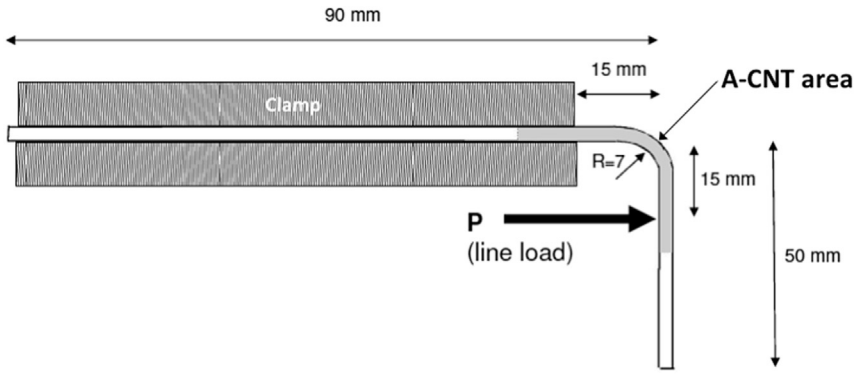

Fig. 2. L-shape bend laminate specimen (with A-CNT reinforced area of 50 mm × 20 mm shown) testing configuration. One side (left in the figure) of the specimen is clamped and load (P) is applied as a line load to the free end of the specimen. All dimensions in mm.

each type of strength testing, following ASTM testing standards except for L-shape bending. 3 specimens each of the baseline and A-CNT reinforced laminates are used in all cases except OHC where 6 specimens of each are used. Tension-bearing testing [40] is one of the available configurations for assessing mechanically fastened composite joints [41], a critical configuration for composites given their relatively poor performance in such 3D load situations relative to metals. Baseline and A-CNT specimens (171 ± 2 mm x 36 ± 0.6) were machined from the same laminate. To avoid hole damage, a 6.0–6.48 mm diameter hole was precision machined 36 mm from the specimen edge. The A-CNT reinforced region extends over the entire hole area (50 mm from the edge, and 36 mm wide). The double shear tension configuration [4] (see Procedure A in ASTM D5961) was utilized with a steel pin through the hole (clearance fit) in the carbon fiber specimen between two steel plates. Two steel washers (12 mm diameter and 1 mm thick) were placed on both sides of the steel pin, and 1 N-m torque was applied to fix the steel pin. Specimens were loaded in displacement control at 0.025 mm/s.

Open hole compression testing (OHC) [42] along with compression after impact (CAI), are relevant substructural strength tests that pose particular issues for layered composite materials due to delamination formation and propagation, and are commonly employed in composite assessment [43] For the OHC testing herein, a 6.0–6.48 mm diameter central hole was precision machined as described above in 220 ± 2 mm x 24.0 ± 0.5 mm specimens. In the case of the A-CNT specimens, 30 mm × 24 mm wide A-CNTs forests were placed at all interfaces centered on the hole. Following the ASTM Standard, specimens were supported against buckling between two 125 mm flat platens that each contain a center 20 mm diameter hole. Specimens are clamped with a gage length of 130 mm and loaded in compression at 0.025 mm/s.

The last substructural strength test employs an L-shaped bend configuration that is common in industry (*e.g.,* see Ref. [44]) due to the significant complexity of this type of loading including mode mixity. The primary motivation for this L-shape study is evaluation of the processibility of an A-CNT reinforced laminate into an aerospace application-relevant small-radius (relative to specimen thickness) corner L-shape. Planar laminates (220 × 200 mm^2) were bent 90° (7 mm of radius of curvature) prior to curing on a steel tool with moderate heating (65 °C) [4]. The specimen was trimmed to a 20 mm width. For the nano-stitched specimens, the CNT region (50 × 20 mm^2) was centered on the bent section of the specimen as can be seen in Fig. 2. For testing, one side (left in Fig. 2) of the specimen was clamped and a linear load was applied at a 15 mm offset to the free side of the specimen at 0.083 mm/s until the specimen failed. This is a common industry configuration but does not follow the ASTM D6415 Standard curved beam inter-laminar tensile stress (ILTS) configuration that attempts to isolate interlaminar tensile failure; rather, the test here creates a complex interlaminar stress state involving at least both tension and shear, as encountered in application practice.

3. Results and discussion

The reinforcing effect of the A-CNTs at the ply interfaces is expected through both load sharing across the interface by the nanofibers to the first layer of microfibers in each ply, and toughening of the matrix. The A-CNTs comprise in excess of 10^9 fibers/cm^2 of laminate interface. Long CNTs (20 μm) as used here give ~ 1200 cm^2 of surface area in a cm^2 of laminate. This compares to ~800 cm^2 of surface area from all the carbon fibers in all plies of the 16-ply laminate; thus, the amount of fiber (CNT) surface area due to the A-CNTs at each interface is on the same order as all the surface area from all the carbon microfibers in the laminate. As stated earlier, although 20 μm A-CNTs are added to each interface (15 interfaces in a 16-ply laminate), the overall thickness (2.08 mm) of the baseline and A-CNT specimens are the same. Furthermore, extensive scanning electron microscopy (SEM) analysis reveals that the interlaminar region thickness is not changed (see Fig. 3). As can be seen in exemplary micrographs in Fig. 3, the A-CNTs are compressed in some regions, and generally fill matrix-rich regions between adjacent fibers in plies above and below the interface. Thus, the A-CNTs interpenetrate the adjacent plies and do not create an increased-thickness interlayer compared to the baseline laminates. In interpreting the strength data reported, herein a larger interlayer (which is not observed) would generally result in decreased stiffness and strength due to the loss of microfiber volume fraction, or potentially introduce additional process-zone toughening in the same way as compliant interleaves [45,46]. Results across all three types of strength testing are summarized in Table 1, showing (where the data is statistically significant) increases in all properties measured, and in some cases (such as the critical bearing strength) relatively large improvements.

Interface reinforcement and its effects on in-plane strength are clearly evident in the bearing stress-strain results from the tension-bearing strength tests in Fig. 4 which contains exemplary bearing stress-strain curves for baseline and A-CNT specimens: baseline specimens have a load drop at ~550 MPa (a little over half of ultimate strength), whereas the A-CNT specimens do not. The load drop is typical of this laminate in this loading configuration and is a result of a large shear-dominated delamination forming between the outer 0° and 90° plies. Such failure has been studied both experimentally and numerically, *e.g.,* [47] due to its importance in sizing and design of aerospace bolted joints. The load drop is not

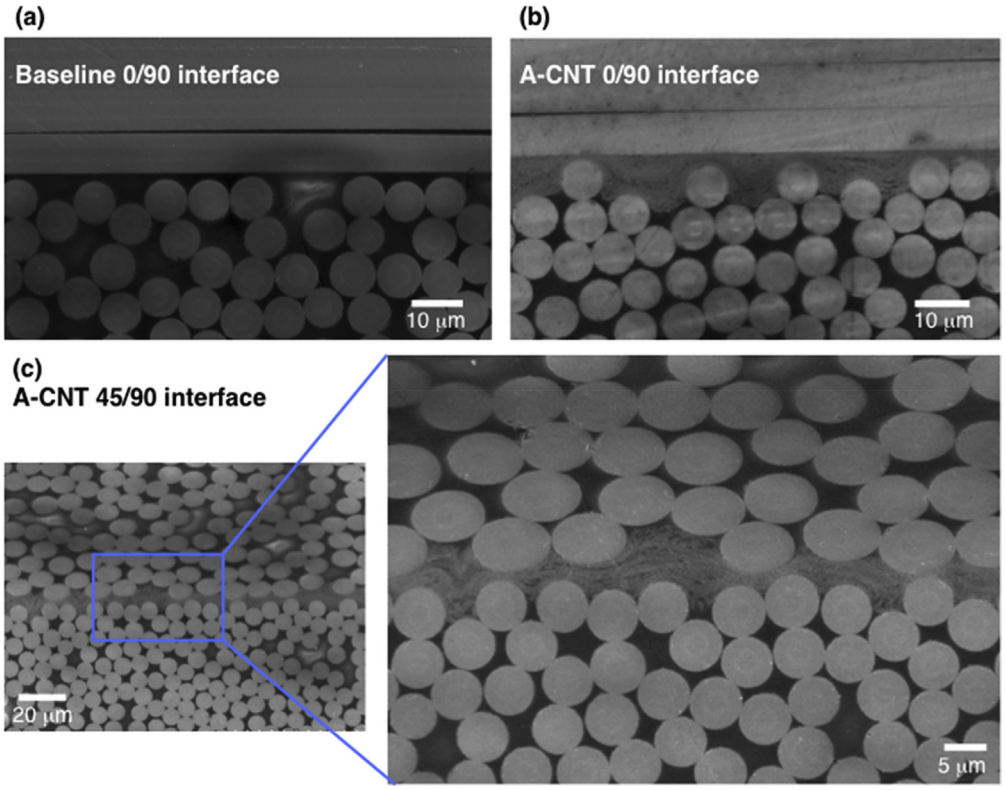

Fig. 3. Representative scanning electron micrographs of ply interfaces: (*a*) 0/90 interface of a baseline specimen, (*b*) A-CNT reinforced 0/90 interface with aligned CNTs visible as light grey area around 90° fibers in lower ply, (*c*) A-CNT reinforced 45/90 interface showing the A-CNTs bridging the first layer of microfibers in both plies.

Table 1
Strength testing summary data.

	Baseline	A-CNT	Change
Tension bearing			
Chord modulus (GPa)	5.29 ± 0.03	5.375 ± 0.006	+1.7%
Critical bearing strength (MPa)	548 ± 4	720 ± 30	+30%
Ultimate bearing strength (MPa)	979 ± 32	977 ± 13	−0.3%
Open hole compression			
Ultimate strength	292 ± 5	333 ± 6	+14%
L-shape bend			
Ultimate load (N)	430 ± 11	430 ± 3	0.0%
Deflection at break (mm)	7.8 ± 0.7	9.8 ± 1.3	+26%
Energy to break (N × m)	2.6 ± 0.3	3.4 ± 0.5	+31%

observed for the A-CNT reinforced specimens and is interpreted as a suppression of the delamination. Increased compliance in this region and slightly above is observed for the A-CNT reinforced specimens indicating damage formation, but again there are no large load drops; this is likely a result of interlaminar or intralaminar matrix damage, but is not associated with the aforementioned delamination propagation due to the lack of observed loss of load carrying capability. As a result, the critical bearing strength is increased significantly. The ultimate strength does not change (within statistical significance) between the baseline and A-CNT specimens, which is attributed to the ultimate strength being dominated by in-plane microfiber failure. Thus, pre-ultimate damage in the interlaminar region is suppressed by the A-CNT

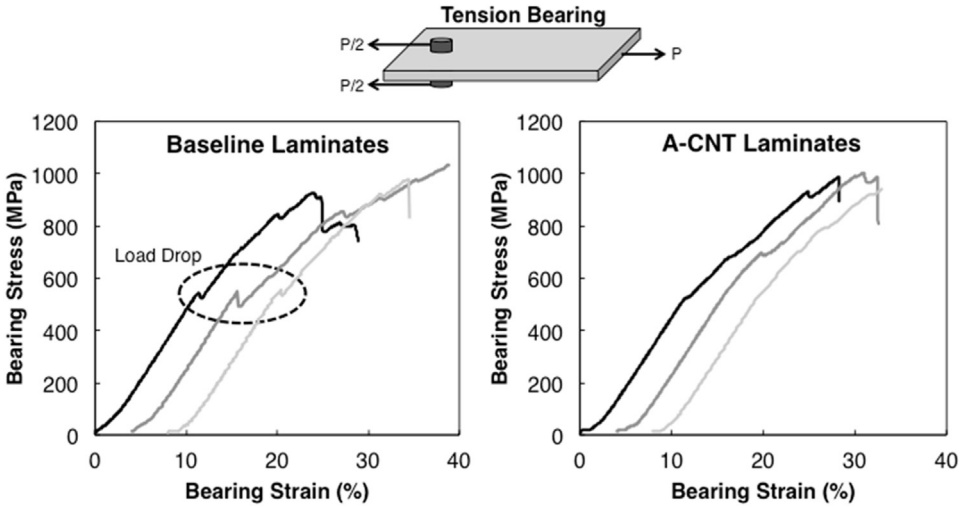

Fig. 4. Bearing stress-strain curves for tension-bearing tests. For comparative purposes, the curves of the different specimens are offset on the x axis.

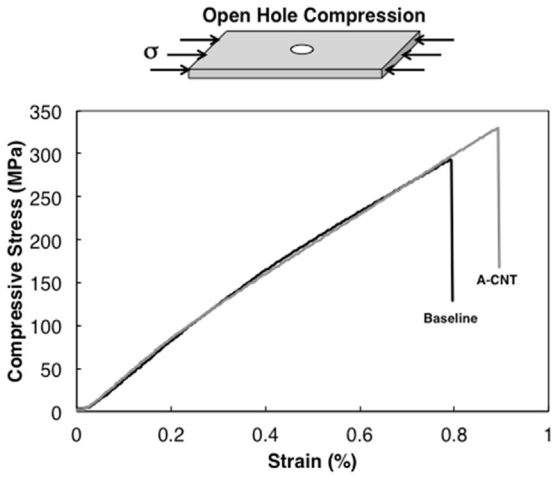

Fig. 5. Representative stress-strain curves for open hole compression (OHC) tests at median values of strength.

reinforcement giving an increase in the useful strength of the composite laminate. It is interesting to compare the results here with algned-CNT reinforcement from a fuzzy-fiber hierarchical architecture [35] also tested in tension-bearing. In the fuzzy-fiber architecture, aligned CNTs are grown on woven microfibers, and both the interlaminar and intralaminar regions are reinforced. In that work, the chord modulus, critical bearing strength, and ultimate strength were all increased with a clear change in the mode of failure from shear dominated "Bearing" to microfiber dominated "Lateral (Net Tension)" as described by the ASTM Standard. The chord modulus also increased significantly, all indicating that aligned CNTs in the intralaminar and interlaminar regions altered significantly the bearing response. Here, however, the interlaminar-only A-CNT reinforcement changed the pre-ultimate failure mode, increased chord modulus slightly (by 1.5%, but significantly), but did not change ultimate failure as no change in the mode of failure (the Bearing failure mode [40] was observed in all cases). This is consistent with the effect of the A-CNTs being restricted solely to interlaminar-region involved modes of failure.

Open hole compression (OHC) testing, as discussed earlier, is a common sub-structural composite strength test that reveals weak attributes of laminated composites, namely susceptibility to delamination and sub-laminate buckling. An initial round of testing which showed a significant 10% increase in ultimate OHC strength motivated the more extensive study presented here. Median (based on ultimate strength) loading curves are shown in Fig. 5 for both baseline and A-CNT specimens. For all specimens tested, the form of the curves is self-similar with a load softening in the range of 100–150 MPa, attributed to the onset and growth of different damage modes local to the hole. In all cases, *post-mortem* visual inspection of the failure is likewise the same across both specimen types. The damage is characterized as "MGM" failure following the ASTM Standard [42] since the laminates exhibit multiple modes of failure (sublaminate buckling etc.) at the hole. As noted in Table 1, a significant 14% increase in ultimate compressive strength was observed and is attributed to an increase in the strength and toughness of the mixed-mode loaded lamina interfaces.

L-shape bend tests were also performed following an investigation that looked primarily at forming the A-CNT forests over tight-radius (7 mm radius) corners. Baseline and A-CNT laminates are found to have the same thickness and quality in the L bend region, and both failed at the same load during testing (~450 N). Exemplary load-deflection curves are shown in Fig. 6 along with microscopy at different scales revealing CNTs pulled out of failed interlamainar regions. As in the tension-bearing and OHC tests, the A-CNTs seem to suppress critical pre-failure modes, increasing the deflection at failure of the A-CNT specimens by a significant 26% relative to the reference specimens (see Table 1). This translates into increased energy to break the specimen as tabulated in Table 1.

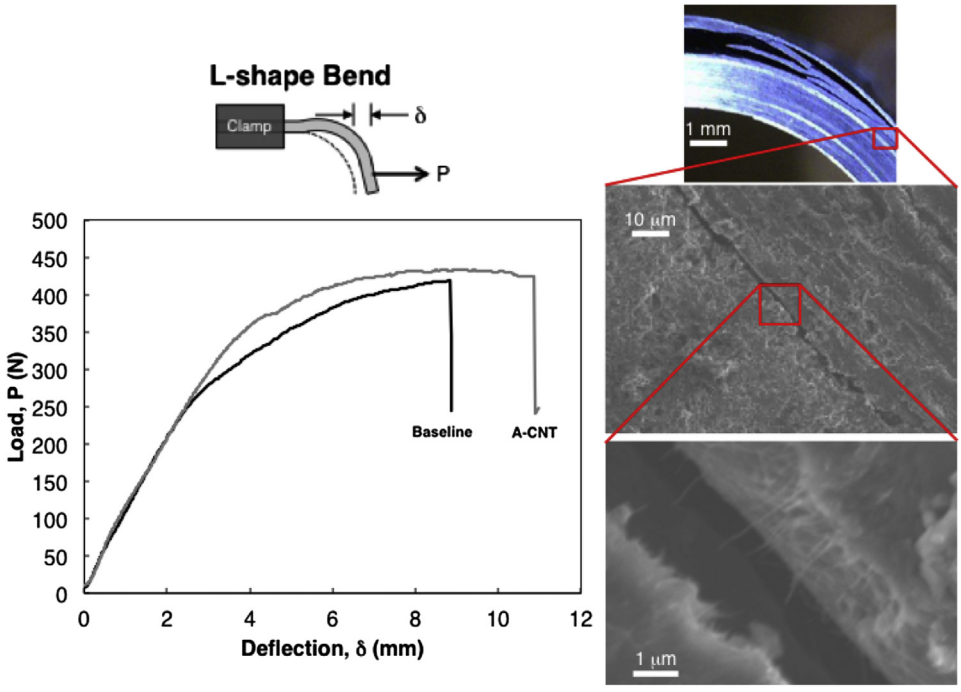

Fig. 6. L-shape bend test results: (left) Representative load-deflection curves at median values of strength, and (right) micrographs of a broken A-CNT reinforced interface showing multi-micron long CNTs pulled out of the polymer matrix.

Nonlinear deformation for these L-shape bend tests, due to the higher deflections associated with the A-CNT specimens, suggests that higher interlaminar stresses are resisted by the A-CNT reinforced interfaces. As with the tension-bearing and OHC tests completed to date, follow-up work for the L-shape bend testing would be to model (via finite element analysis) the level of interlaminar stresses resisted by the A-CNT specimens to assess the strengthening effect and also to ascertain the level to stop testing before ultimate load is reached to explore the extent of damage before ultimate failure, in order to understand differences in the extent and mode of damage between reinforced and A-CNT specimens. Microscopy of the L-region of a nano-stitched specimen reveals aligned CNTs that were pulled out from the interfaces of the micro-cracks produced during the tests (see Fig. 6). Although the A-CNTs are around 20 μm in length, only 2–3 μm are pulled out from the polymer matrix. It is not possible to assess the failure mode of the CNTs, *i.e.,* pull-out, mixed mode, etc. Similar behavior has been observed in Mode I testing of A-CNT reinforced laminates and fuzzy-fiber composites [35].

4. Conclusions and recommendations

Nanoengineered aerospace-grade composites were developed by placing z-direction A-CNTs across each ply-ply interface to effectively stitch the plies together. Substructural strength tests reveal clear differences in pre-ultimate and ultimate strength response, most notably in tension-bearing and open hole compression tests, *e.g.,* suppression of delamination damage in the tension-bearing tests clearly alters the load-deflection curve by removing the large load drop associated with delamination formation. The A-CNTs physically bridge and reinforce across the ply-ply interfaces, improving interlaminar properties and arresting pre-ultimate failure modes. In all the tests done in this study, the A-CNT reinforced composites showed significantly better performance than the baseline specimens. Aligned nanofibers, particularly the A-CNTs used here, are a promising reinforcement that improves the interlaminar properties of the laminates, leading to enhanced substructural laminate strength, and also adding multi-functionality (such as damage sensing, and heating [48–51]).

The results presented here have clear experimental and modeling next steps, including expanding the data-set to allow A- and B-basis values to be established so that these nanoengineered laminates can be considered for structural applications. Additional strength tests are also warranted, such as compression after impact (CAI), impact damage resistance, fatigue, and hot-wet loading in various configurations. Indeed, recent work introducing unaligned and magnetically-aligned CNTs into the bulk matrix of woven laminated composites has shown promise in terms of fatigue response at the laminate level [52,53]. Last, detailed mechanistic understanding of the altered damage progression in these laminates needs to be further clarified via model-experiment correlation studies, *e.g.,* [54]. Because the increases in strength observed in this work are in the context of highly three-dimensional loadings, and therefore are due to both strengthening and toughening mechanisms, both need to be elucidated. Multi-scale modeling (*e.g.,* [55–57]) of mechanisms clarified by experimental testing will help build a needed predictive damage tolerance capability. Given the large increases in strength observed herein for aerospace laminates, it may be possible to remove the long-standing Achilles heel of weak interfaces in laminated composites.

Acknowledgments

This work was supported by Airbus, Boeing, Embraer, Lockheed Martin, Saab AB, Spirit AeroSystems Inc., Textron Systems, ANSYS, Hexcel, and TohoTenax through MIT's Nano-Engineered Composite aerospace STructures (NECST) Consortium. The authors thank Sunny Wicks (MIT), John Kane (MIT) and the entire necstlab at MIT for technical support and advice, Diana Lewis (MIT) for assistance with data reduction and interpretation, Itai Stein (MIT) for technical advice and A-CNT forest imaging, and Kyoko Ishiguro (MIT) for assistance with specimen fabrication. This work was carried out in part through the use of MIT's Microsystems Technology Laboratories and supported in part by the U. S. Army Research Laboratory and the U. S. Army Research Office through the Institute for Soldier Nanotechnologies, under contract number W911NF-13-D-0001.

References

[1] L. Tong, A.P. Mouritz, M. Bannister, 3D Fibre Reinforced Polymer Composites, Elsevier, Oxford, 2002.
[2] K.A. Dransfield, L.K. Jain, Y.-W. Mai, On the effects of stitching in CFRPs-I. mode I delamination toughness, Compos. Sci. Technol. 58 (1998) 815–827.
[3] A.P. Mouritz, K.H. Leong, I. Herszberg, A review of the effect of stitching on the in-plane mechanical properties of fibre-reinforced polymer composites, Compos. Part A 28 (1997) 979–991.
[4] R. Guzman de Villoria, L. Ydrefors, P. Hallander, K. Ishiguro, P. Nordin, B.L. Wardle, Aligned carbon nanotube reinforcement of aerospace carbon fiber composites: substructural strength evaluation for aerostructure applications, in: 53rd AIAA/ASME/ASCE/AHS/ASC Structures, Structural Dynamics and Materials Conference, 2012.
[5] L. Liu, W. Ma, Z. Zhang, Macroscopic carbon nanotube assemblies: preparation, properties, and potential applications, Small 7 (2011) 1504–1520.
[6] L. Sun, H.J. Sue, Epoxy/carbon Nanotube Nanocomposites, John Wiley & Sons Inc., USA, 2010.
[7] E. Bekyarova, E.T. Thostenson, A. Yu, M.E. Itkis, D. Fakhrutdinov, T.-W. Chou, R.C. Haddon, Functionalized single-walled carbon nanotubes for carbon fiber-epoxy composites, J. Phys. Chem. C 111 (2007) 17865–17871.
[8] M. Kim, Y.-B. Park, O.I. Okoli, C. Zhang, Processing, characterization, and modeling of carbon nanotube-reinforced multiscale composites, Compos. Sci. Technol. 69 (2009) 335–342.
[9] P.R. Thakre, D.C. Lagoudas, J.C. Riddick, T.S. Gates, S.-J.V. Frankland, J.G. Ratcliffe, J.J. Zhu, E.V. Barrera, Investigation of the effect of single wall carbon nanotubes on interlaminar fracture toughness of woven carbon fiber-epoxy composites, J. Compos. Mater. (2011), 21998310389088.
[10] R.J. Mora, J.J. Vilatela, A.H. Windle, Properties of composites of carbon nanotube fibres, Compos. Sci. Technol. 69 (2009) 1558–1563.
[11] H. Qian, E.S. Greenhalgh, M.S.P. Shaffer, A. Bismarck, Carbon nanotube-based hierarchical composites: a review, J. Mater. Chem. 20 (2010) 4751–4762.
[12] R. Van Noorden, Chemistry: the trials of new carbon, Nat. News 469 (2011) 14–16.
[13] M.F. De Volder, S.H. Tawfick, R.H. Baughman, A.J. Hart, Carbon nanotubes: present and future commercial applications, Science 339 (2013) 535–539.
[14] F.H. Gojny, M.H.G. Wichmann, U. Köpke, B. Fiedler, K. Schulte, Carbon nanotube-reinforced epoxy-composites: enhanced stiffness and fracture toughness at low nanotube content, Compos. Sci. Technol. 64 (2004) 2363–2371.
[15] S. Chandrasekaran, N. Sato, F. Tölle, R. Mülhaupt, B. Fiedler, K. Schulte, Fracture toughness and failure mechanism of graphene based epoxy composites, Compos. Sci. Technol. 97 (2014) 90–99.
[16] L.C. Herrera-Ramírez, P. Castell, J.P. Fernández-Blázquez, A. Fernández, R. Guzman de Villoria, How do graphite nanoplates affect the fracture toughness of polypropylene composites? Compos. Sci. Technol. 111 (2015) 9–16.
[17] T.H. Hsieh, A.J. Kinloch, A.C. Taylor, I.A. Kinloch, The effect of carbon nanotubes on the fracture toughness and fatigue performance of a thermosetting epoxy polymer, J. Mater. Sci. 46 (2011) 7525–7535.
[18] N. Lachman, Y. Harel, A. Green, N. Iuster, J.-P. Lellouche, H.D. Wagner, Effect of scale and surface chemistry on the mechanical properties of carbon nanotubes-based composites, J. Polym. Sci. B 50 (2012) 957–962.
[19] J.H. Koo, Polymer Nanocomposites, McGraw-Hill Professional Pub, 2006.
[20] P.M. Ajayan, J.M. Tour, Materials science: nanotube composites, Nature 447 (2007) 1066–1068.
[21] M. Quaresimin, K. Schulte, M. Zappalorto, S. Chandrasekaran, Toughening mechanisms in polymer nanocomposites: from experiments to modelling, Compos. Sci. Technol. (2015).
[22] T.-W. Chou, L. Gao, E.T. Thostenson, Z. Zhang, J.-H. Byun, An assessment of the science and technology of carbon nanotube-based fibers and composites, Compos. Sci. Technol. 70 (2010) 1–19.
[23] Z. Spitalsky, D. Tasis, K. Papagelis, C. Galiotis, Carbon nanotube–polymer composites: chemistry, processing, mechanical and electrical properties, Prog. Polym. Sci. 35 (2010) 357–401.
[24] M.J. Green, N. Behabtu, M. Pasquali, W.W. Adams, Nanotubes as polymers, Polymer 50 (2009) 4979–4997.
[25] E.T. Thostenson, C. Li, T.-W. Chou, Nanocomposites in context, Compos. Sci.

Technol. 65 (2005) 491–516.
[26] J.N. Coleman, U. Khan, W.J. Blau, Y.K. Gun'ko, Small but strong: a review of the mechanical properties of carbon nanotube-polymer composites, Carbon 44 (2006) 1624–1652.
[27] P. Ajayan, P. Braun, L. Schadler, Nanocompos. Sci. Technol. (2003).
[28] K. Schulte, A.H. Windle, Compos. Sci. Technol. 67 (2007) 777, 5, April.
[29] R.A. Vaia, H.D. Wagner, Framework for nanocomposites, Mater. Today (2004) 32–37.
[30] M.A. Arca, D. Coker, Experimental investigation of CNT effect on curved beam strength and interlaminar fracture toughness of CFRP laminates, in: Journal of Physics: Conference Series, vol. 524, IOP Publishing, 2014. No. 1.
[31] S.U. Khan, J.-K. Kim, Impact and delamination failure of multiscale carbon nanotube-fiber reinforced polymer composites, Int. J. Aeronaut. Space Sci. 12 (2011) 115–133.
[32] G. Lubineau, A. Rahaman, A review of strategies for improving the degradation properties of laminated continuous-fiber/epoxy composites with carbon-based nanoreinforcements, Carbon 50 (2012) 2377–2395.
[33] E.J. Garcia, B.L. Wardle, A.J. Hart, Joining prepreg composite interfaces with aligned carbon nanotubes, Compos. Part Appl. Sci. Manuf. 39 (2008) 1065–1070.
[34] J. Blanco, E.J. Garcia, R. Guzman de Villoria, B.L. Wardle, Limiting mechanisms in mode I interlaminar toughness of composites reinforced with aligned carbon nanotubes, J. Compos. Mater. 43 (2009) 825–841.
[35] S.S. Wicks, R. Guzman de Villoria, B.L. Wardle, Interlaminar and intralaminar reinforcement of composite laminates with aligned carbon nanotubes, Compos. Sci. Technol. 70 (2010) 20–28.
[36] H. Suemasu, H. Takahashi, T. Ishikawa, On failure mechanisms of composite laminates with an open hole subjected to compressive load, Compos. Sci. Technol. 66 (2006) 634–641.
[37] Y. Li, M. Li, Y. Gu, Z. Zhang, Numerical, Experimental, Study on the effect of lay-up type and structural elements on thickness uniformity of L-shaped laminates, Appl. Compos. Mater. 16 (2009) 101–115.
[38] A.J. Hart, A.H. Slocum, Rapid growth and flow-mediated nucleation of millimeter-scale aligned carbon nanotube structures from a thin-film catalyst, J. Phys. Chem. B 110 (2006) 8250–8257.
[39] B.L. Wardle, D.S. Saito, E.J. García, A.J. Hart, R.G. de Villoria, E.A. Verploegen, Fabrication and characterization of ultrahigh-volume- fraction aligned carbon nanotube–polymer composites, Adv. Mater. 20 (2008) 2707–2714.
[40] ASTM D 5961/D 5961–01 e1, Standard Test Method for Bearing Response of Polymer Matrix Composites Materials, ASTM International, 2003.
[41] S.D. Thoppul, J. Finegan, R.F. Gibson, Mechanics of mechanically fastened joints in polymer-matrix composite structures – a review, Compos. Sci. Technol. 69 (2009) 301–329.
[42] ASTM D6484/D6484M – 14, Test Method for Open-hole Compressive Strength of Polymer Matrix Composite Laminates, ASTM International, 2014.
[43] D.F. Adams, L.A. Carlsson, R.B. Pipes, Experimental Characterization of Advanced Composite Materials, CRC Press, Boca Raton, 2003.
[44] B. Gözlüklü, D. Coker, Modeling of the dynamic delamination of L-shaped unidirectional laminated composites, Compos. Struct. 94 (2012) 1430–1442.
[45] N. Sela, O. Ishai, Interlaminar fracture toughness and toughening of laminated composite materials: a review, Composites 20 (1989) 423–435.
[46] T.K. Tsotsis, Interlayer toughening of composite materials, Polym. Compos. 30 (2009) 70–86.
[47] Z. Kapidžić, H. Ansell, J. Schön, K. Simonsson, Quasi-static bearing failure of CFRP composite in biaxially loaded bolted joints, Compos. Struct. 125 (2015) 60–71.
[48] C. Li, E.T. Thostenson, T.-W. Chou, Sensors and actuators based on carbon nanotubes and their composites: a review, Compos. Sci. Technol. 68 (2008) 1227–1249.
[49] R. Guzman de Villoria, N. Yamamoto, A. Miravete, B.L. Wardle, Multi-physics damage sensing in nano-engineered structural composites, Nanotechnology 22 (2011) 185502.
[50] S.T. Buschhorn, N. Lachman, J. Gavin, B.L. Wardle, S.S. Kessler, G. Thomas, Buschhorn, Electrothermal icing protection of aerosurfaces using conductive polymer nanocomposites, in: 54th AIAA/ASME/ASCE/AHS/ASC Structures, Structural Dynamics, and Materials Conference, 2013.
[51] J. Lee, I.Y. Stein, S.S. Kessler, B.L. Wardle, Aligned carbon nanotube film enables thermally induced state transformations in layered polymeric materials, ACS Appl. Mater. Interfaces 7 (2015) 8900–8905.
[52] J.S. Fenner, I.M. Daniel, Hybrid nanoreinforced carbon/epoxy composites for enhanced damage tolerance and fatigue life, Compos. Part A 65 (2014) 47–56.
[53] C. Ma, H.-Y. Liu, X. Du, L. Mach, F. Xu, Y.-W. Mai, Fracture resistance, thermal and electrical properties of epoxy composites containing aligned carbon nanotubes by low magnetic field, Compos. Sci. Technol. 114 (2015) 126–135.
[54] M. Quaresimin, M. Salviato, M. Zappalorto, Toughening Mechanisms in Composite Materials, Woodhead, Cambridge, 2015.
[55] C. Soutis, P.W. Beaumont, Multi-scale Modelling of Composite Material Systems: the Art of Predictive Damage Modelling, Woodhead, Cambridge, 2005.
[56] J. Jancar, J.F. Douglas, F.W. Starr, S.K. Kumar, P. Cassagnau, A.J. Lesser, S.S. Sternstein, M.J. Buehler, Current issues in research on structure–property relationships in polymer nanocomposites, Polymer 51 (2010) 3321–3343.
[57] P.P. Camanho, C.G. Dávila, S.T. Pinho, J.J.C. Remmers (Eds.), Mechanical Response of Composites, vol. 10, Springer Science & Business Media, Netherlands, 2008.